

Searching for turbulence models by artificial neural network

Masataka Gamahara

Graduate School of Information Sciences, Tohoku University, Sendai 980-8579, Japan

Yuji Hattori*

Institute of Fluid Science, Tohoku University, Sendai 980-8577, Japan

(Received 23 June 2016; published 4 May 2017)

An artificial neural network (ANN) is tested as a tool for finding a new subgrid model of the subgrid-scale (SGS) stress in large-eddy simulation. An ANN is used to establish a functional relation between the grid-scale flow field and the SGS stress without any assumption of the form of function. Data required for training and test of the ANN are provided by direct numerical simulation of a turbulent channel flow. It is shown that an ANN can establish a model similar to the gradient model. The correlation coefficients between the real SGS stress and the output of the ANN are comparable to or larger than similarity models, but smaller than a two-parameter dynamic mixed model. Large-eddy simulations using the trained ANN are also performed. Although ANN models show no advantage over the Smagorinsky model, the results confirm that the ANN is a promising tool for establishing a new subgrid model with further improvement.

DOI: [10.1103/PhysRevFluids.2.054604](https://doi.org/10.1103/PhysRevFluids.2.054604)

I. INTRODUCTION

Large-eddy simulation (LES) is used as an important tool of numerical simulation in a wide variety of fields where turbulent flows appear. In LES the turbulent flow fields are decomposed into resolved-scale or grid-scale (GS) flow field and small-scale or subgrid-scale (SGS) fluctuations by a filtering operation. In incompressible turbulent flows the effects of the fluctuations on the GS flow field appear as the residual or SGS stress tensor. How to model the SGS stress tensor using the GS flow field is the most important issue in LES.

A number of subgrid models have been proposed since the Smagorinsky model [1]. Most of them are categorized into the Smagorinsky model, the similarity model [2], and the gradient model [3]; there are also dynamic versions of these models [4,5] and mixed models [6] (see, e.g., Lesieur and Métais [7] and Meneveau and Katz [8] for reviews). The performance of these models has been tested for some particular flows like isotropic turbulence [9] and mixing layers [10]. There is no model which is better than the other models in any flows, although the dynamic and mixed models often give more accurate results than nondynamic models. The Smagorinsky model is too dissipative, allowing no backward scatter of SGS energy into the grid scale; in contrast, the similarity model gives too much backward scatter and is not sufficiently dissipative. The gradient model is correct in the limit of small grid size but known to be unstable as it is not sufficiently dissipative. Improvement of these models by, e.g., dynamic procedure is often accompanied by increasing numerical costs. The accuracy of the results obtained by LES is still limited as they should be interpreted with much care when experimental or direct numerical simulation (DNS) results are unavailable for validation; controversially, however, this is the very situation in which LES is most wanted. Thus, a new subgrid model which is much better than the existing ones should be developed. In order to pursue such a subgrid model essentially new ideas of modeling would be required; however, there has been no such idea since the prototypes of the above models were proposed.

The final goal of our research is to establish a new subgrid model for the SGS stress which performs better than the existing models. This is not an easy task since there are potentially a huge

*Corresponding author: hattori@fmail.ifs.tohoku.ac.jp

number of possibilities of modeling. In principle one can use the GS flow field in the whole domain to express the SGS stress at one point as in nonlocal methods in Reynolds-averaged Navier-Stokes modeling [11]; the history of the GS flow field may also be used as in the Reynolds stress transport model [12]. On the other hand, the subgrid model should be based on physics of turbulence and it seems difficult to invent an essentially new model after the models listed above were established with much effort. However, the methods of machine learning, which are extensively and successfully used in many areas, can provide us a tool for going beyond the ability of human thought; they are useful if they can automatically extract the essential GS flow field required for accurate modeling. In this paper, we test whether the artificial neural network (ANN), which is one of the methods of machine learning, can be used for finding a subgrid model; it is a first step toward the above goal.

There have been many applications of ANNs to turbulence modeling. Sarghini *et al.* [13] used an ANN to find a relation between the GS flow field and the turbulent viscosity coefficient in the mixed model. Moreau *et al.* [14] used an ANN to estimate the subgrid variance in the Cook-Riley model for a scalar field in isotropic turbulence. Recently an ANN was used by Ma *et al.* [15] to find closure terms for a one-dimensional model of bubbly multiphase flows. There are many applications of ANNs to combustion [16–19]; an ANN is used to speed up subgrid chemistry computations, which are usually the bottleneck of LES of turbulent flames. In plasma turbulence Citrin *et al.* [20] used an ANN to construct a model for a tokamak turbulence transport model. In most of these works, however, an ANN was used only as a complementary tool for optimizing model constants. Moreover, few works have dealt with SGS stress arising from convective terms, which is intrinsic to turbulence. In other words, there has been no attempt to construct an essentially new subgrid model of the SGS stress using an ANN.

It should be pointed out that we aim at establishing a functional relation between the GS flow field and the SGS stress tensor without any assumption on its form; this has not been done in the past. It is contrasted to the approach by Sarghini *et al.* [13], who assumed the relation to be the mixed model: their aim was to reduce the computational time by replacing the evaluation of the turbulent viscosity coefficient with an ANN; the training target was the Bardina model instead of the real SGS stress. If the ANN is shown to be an effective tool for turbulence modeling, it can be also applied to complex flows including compressible flows, multi-phase flows, and reactive flows, in which it is not always clear how to model the residual terms.

The paper is organized as follows. Numerical methods are described in Sec. II; after the outline description in Sec. II A, methods of DNS are detailed in Sec. II B. Preparation of data for the ANN is summarized in Sec. II C, and methods of ANNs including the choice of input variables are described in Sec. II D. The results are shown in Sec. III: First, the choice of input variables is discussed in Sec. III A; in Sec. III B, the ANN is shown to be successful in learning the SGS stress. Basic features of learning are shown in Sec. III C, and the applicability of an ANN trained at a low Reynolds number to higher Reynolds numbers is tested in Sec. III D. After investigating what kind of model the ANN has established in Sec. III E, some results of LESs using the trained ANN (*a posteriori* test) are presented in Sec. III F. A summary and discussion of future works are given in Sec. IV.

II. NUMERICAL METHODS

A. Outline

In LES small fluctuations of a flow variable f are filtered out and we are concerned with the resolved-scale or GS flow field $\bar{f} = \int G(\mathbf{x}') f(\mathbf{x} - \mathbf{x}') d\mathbf{x}'$, where G is a filter function. The GS flow field is governed by the filtered Navier-Stokes equations

$$\frac{\partial \bar{u}_i}{\partial t} + \frac{\partial}{\partial x_j} (\bar{u}_i \bar{u}_j) = -\frac{\partial \bar{p}}{\partial x_i} + \frac{1}{\text{Re}} \frac{\partial^2 \bar{u}_i}{\partial x_k \partial x_k} - \frac{\partial \tau_{ij}}{\partial x_j}, \quad (1)$$

$$\frac{\partial \bar{u}_j}{\partial x_j} = 0. \quad (2)$$

TABLE I. Parameter values of DNS.

Re_τ	L_x	L_y	L_z	Δx^+	Δy_{\max}^+	Δz^+	$N_x \times N_y \times N_z$
180	4π	2	2π	11.8	5.4	7.1	$192 \times 128 \times 160$
400	2π	2	π	9.8	7.9	4.9	$256 \times 192 \times 256$
600	2π	2	π	7.4	8.1	3.7	$512 \times 256 \times 512$
800	π	2	π	6.5	7.7	3.3	$384 \times 384 \times 768$

Here the residual or SGS stress tensor

$$\tau_{ij} = \overline{u_i u_j} - \overline{u_i} \overline{u_j} \quad (3)$$

depends not only on the GS flow field but also on fluctuations and should be modeled using the GS flow field.

In the present study we use an ANN to establish a functional relation between the GS flow field and the SGS stress tensor. First, training data for the ANN are prepared using DNS data. The GS flow field is calculated from DNS data and used as input variables of the ANN. The SGS stress tensor is also calculated from DNS data and used as a training target of output variables. Then, the ANN is trained to establish a functional relation between the input and output variables. The ability of the trained ANN is checked using DNS data which are not used in training. The trained ANN is also tested in actual LESs.

B. Direct numerical simulation

The data used for training and test are obtained by DNS of a turbulent channel flow. We use the formulation of Kim *et al.* [21]. For spatial discretization the sixth-order accurate compact scheme is used in y which is the direction normal to the walls, while the Fourier collocation method is used in the streamwise direction x and the spanwise direction z , assuming periodic boundary conditions. Nonuniform grids are adopted in y to resolve the boundary layers. The Poisson equations are solved in the Fourier space where they are decomposed into independent second-order ordinary differential equations for Fourier modes; they are also discretized by the compact scheme and solved accurately and efficiently. The friction Reynolds number is $Re_\tau = u_\tau \delta / \nu = 180, 400, 600,$ and 800 , where $u_\tau = \tau_w^{1/2}$, $\tau_w = (1/Re) \frac{\partial u}{\partial y}$, and $\delta = 1$ is the channel half-width. The size of the numerical domain, $L_x \times L_y \times L_z$, the grid spacings in the wall unit, Δx^+ , Δy_{\max}^+ , and Δz^+ , and the number of grid points, $N_x \times N_y \times N_z$, are listed in Table I.

Validity of the DNS is checked in Fig. 1. The mean flow has a wall-law region and log-law region [Fig. 1(a)]. Figure 1(b) shows fine vortical structures visualized by the isosurface of the second invariant of the deformation tensor, which has been observed in previous works [22–24].

C. Preparing data for training and testing

The data obtained by DNS are used both for training and for testing. In training, field data obtained by DNS are filtered as normally done in LES to give the GS flow field on coarse grids, which are used as input variables; in the present study we use the top-hat filter function. The SGS stress is also calculated using the DNS data and is used as training targets of output variables. The values of the filter size and the number of grid points of the coarse grids are listed in Table II; for the most part they are set to the underlined parameter values $Re_\tau = 180, (\underline{\Delta x^+}, \underline{\Delta y_{\max}^+}, \underline{\Delta z^+}) = (35.3, 9.9, 17.7)$. The components of the SGS stress tensor averaged in the streamwise and spanwise directions are shown in Fig. 2, where the rms amplitudes are also shown. They are in good agreement with the previous results [21].

The amount of data used for training is rather small; typically six positions in the streamwise direction are randomly chosen and the data on the corresponding planes parallel to the yz plane at

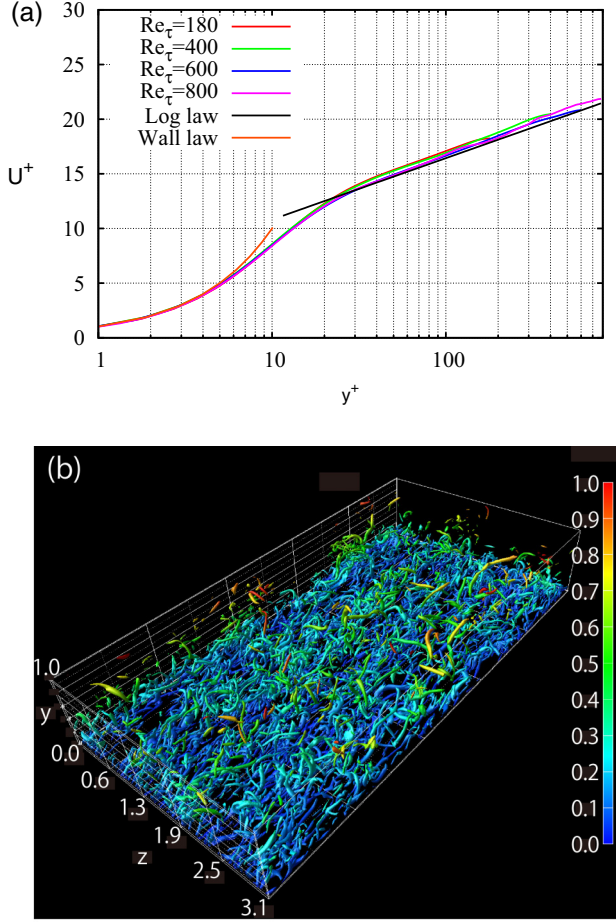


FIG. 1. Results of DNS of channel flow. (a) Mean flow at $Re_\tau = 180, 400, 600,$ and 800 ; (b) vortical structures shown by isosurface of the second invariant Q of the deformation tensor. $Re_\tau = 400, Q = 0.03$.

one instant are used for training. All data at the same instant are used for testing of the trained ANN except for testing the ANN trained at $Re_\tau = 180$ using data at $Re_\tau = 400$ and 800 .

D. Artificial neural network

A feed-forward neural network is employed in establishing a functional relation between the GS flow field and the SGS stress tensor. Figure 3 shows the schematic diagram of the ANN and a single neuron. Let us consider an ANN which consists of L layers. A single neuron of the l th layer receives a set of inputs $\{X_j^{(l-1)}\}$ and then outputs $X_i^{(l)}$ which is calculated as

$$X_i^{(l)} = \mathcal{B}(s_i^{(l)} + b_i^{(l)}), \quad (4)$$

$$s_i^{(l)} = \sum_j W_{ij}^{(l)} X_j^{(l-1)}, \quad (5)$$

where \mathcal{B} is the activation function, $b_i^{(l)}$ is the bias parameter, and $W_{ij}^{(l)}$ is the weight. The bias parameters and the weights are corrected iteratively so that the final output $X^{(L)}$ approximates well the given SGS stress. The data of the first layer $\{X_j^{(1)}\}$ are given by the GS flow field.

TABLE II. Parameter values for filtering. Filter size and number of grid points. They are set to the underlined parameter values for the most part of the paper.

Re_τ	$\overline{\Delta x}^+$	$\overline{\Delta y}_{\max}^+$	$\overline{\Delta z}^+$	$N_x \times N_y \times N_z$
180	41.7	15.6	23.6	$48 \times 48 \times 48$
	43.5	14.5	21.7	$52 \times 52 \times 52$
	<u>35.3</u>	<u>9.9</u>	<u>17.7</u>	<u>$64 \times 64 \times 64$</u>
	23.6	6.0	11.8	$96 \times 96 \times 96$
400	39.3	22.0	19.6	$64 \times 64 \times 64$
	34.3	17.9	17.5	$72 \times 72 \times 72$
	29.9	15.3	15.0	$84 \times 84 \times 84$
	26.2	13.3	13.1	$96 \times 96 \times 96$
600	29.5	33.0	14.7	$128 \times 64 \times 128$
	26.2	26.9	13.1	$144 \times 72 \times 144$
	22.4	23.0	11.2	$168 \times 84 \times 168$
	19.6	19.9	9.8	$192 \times 96 \times 192$
800	26.2	10.9	13.1	$96 \times 256 \times 192$
	19.6	10.9	9.8	$128 \times 256 \times 256$
	13.1	10.9	6.5	$192 \times 256 \times 384$

In the present study the ANN consists of three layers: the input, hidden, and output layers. For simplicity, each independent component of the SGS stress tensor is dealt with separately; in other words, six ANNs are trained to approximate all components of the SGS stress tensor. This point is discussed from the viewpoint of symmetry in the final section. The activation function is the sigmoid function $\mathcal{B}(z) = 1/(1 + e^{-\alpha z})$. The back-propagation is used as a method for training which optimizes the bias parameters and weights iteratively to minimize the difference between the output and the given SGS stress $\sum |X^{(L)} - \tau_{ij}|^2$. The number of neurons of the input layer depends on the choice of input variables as described below, while the output layer consists of a single neuron. The number of neurons of the hidden layer is 100 unless stated explicitly, while the dependence on it is checked in Sec. III C.

We should be careful in choosing the input variables since it is important for effective and successful learning. Although there are many possibilities for the combination of input variables, we limit ourselves to pointwise correspondence between the input and output variables; namely, in order to approximate the SGS stress at one point the GS data at the same point are used as input

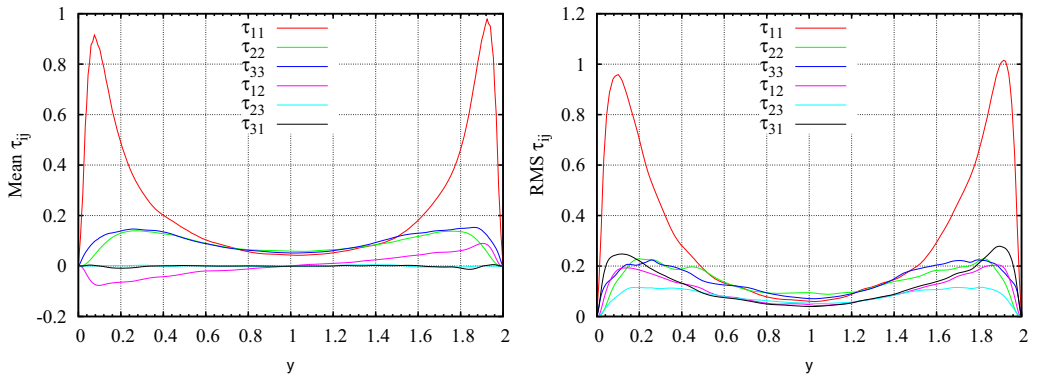


FIG. 2. Distributions of SGS stress tensor τ_{ij} averaged in streamwise and spanwise directions (xz plane). $Re_\tau = 180$, $(\overline{\Delta x}^+, \overline{\Delta y}_{\max}^+, \overline{\Delta z}^+) = (35.3, 9.9, 17.7)$. Average (left) and rms (right) amplitude of fluctuation.

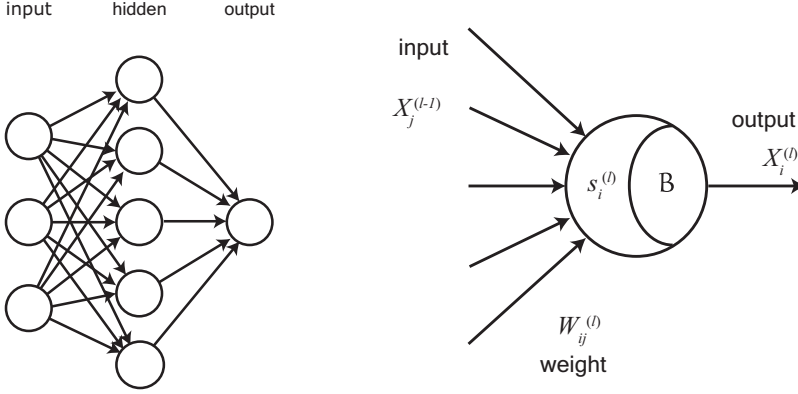


FIG. 3. Schematic diagram of the ANN. Left, network structure; right, single neuron.

variables. We test four sets of input variables: (i) $\{S, y\}$, (ii) $\{S, \Omega, y\}$, (iii) $\{\nabla \bar{\mathbf{u}}, y\}$, and (iv) $\{\nabla \bar{\mathbf{u}}\}$, where $S = [\nabla \bar{\mathbf{u}} + (\nabla \bar{\mathbf{u}})^T]/2$ and $\Omega = [\nabla \bar{\mathbf{u}} - (\nabla \bar{\mathbf{u}})^T]/2$. The first set can give the Smagorinsky model $\tau_{ij} = -2C_S \bar{\Delta}^2 (2S_{kl}S_{kl})^{1/2} S_{ij} + (1/3)\tau_{kk}\delta_{ij}$, while the position y is included to take account of possible dependence on the wall-normal direction. The GS vorticity is added in the second set since it improves the accuracy of the SGS model in some flows [25]. The third set is equivalent to the second one in the sense that $\nabla \bar{\mathbf{u}} = S + \Omega$; in practice, however, the results of learning can be different. The last set is included to check the role of the position y .

III. RESULTS

A. Choice of input variables

First, we investigate which set of input variables results in successful learning. Figure 4 shows correlation coefficients between the SGS stress $\tau_{ij}^{(\text{DNS})}$ calculated using DNS data and $\tau_{ij}^{(\text{ANN})}$ predicted by the trained ANN for the four sets of input variables for $\text{Re}_\tau = 180$, $(\overline{\Delta x^+}, \overline{\Delta y_{\text{max}}^+}, \overline{\Delta z^+}) = (35.3, 9.9, 17.7)$. The correlation coefficients are calculated by integrating in x and z directions:

$$\text{C.C.}(y) = \frac{\langle (\tau_{ij}^{(\text{DNS})} - \langle \tau_{ij}^{(\text{DNS})} \rangle_{xz}) (\tau_{ij}^{(\text{ANN})} - \langle \tau_{ij}^{(\text{ANN})} \rangle_{xz}) \rangle_{xz}}{[\langle (\tau_{ij}^{(\text{DNS})} - \langle \tau_{ij}^{(\text{DNS})} \rangle_{xz})^2 \rangle_{xz}]^{1/2} [\langle (\tau_{ij}^{(\text{ANN})} - \langle \tau_{ij}^{(\text{ANN})} \rangle_{xz})^2 \rangle_{xz}]^{1/2}},$$

$$\langle f \rangle_{xz} = \frac{1}{L_x L_z} \int_0^{L_x} dx \int_0^{L_z} dz f(x, y, z).$$

High correlation implies successful learning. It is seen that learning is most successful when $\{\nabla \bar{\mathbf{u}}, y\}$ are used as input variables as the averaged correlation coefficient $\overline{\text{C.C.}} = (1/L_y) \int_0^{L_y} dy \text{C.C.}(y)$ exceeds 0.7 for all six components as shown in Table III, although $\{\nabla \bar{\mathbf{u}}\}$ gives comparable success; the difference of the correlation coefficients between the two sets is $0 \sim 4\%$. Thus the distance from the wall is not important very much. The Smagorinsky type $\{S, y\}$ gives poor results as the averaged correlation coefficient exceeds 0.7 for only one component τ_{11} ; the correlation coefficients of the other components are small in the entire region except that it is large for τ_{31} near the wall. This result is reasonable since it is known that the eddy-viscosity-type model has little correlation with the real SGS stress [26]. There is a little improvement by including Ω because the set $\{S, \Omega, y\}$ gives three correlation coefficients which exceed 0.7; the correlation coefficients of τ_{33} , τ_{23} , and τ_{31} are small in the central region where both the average and rms amplitudes of these components are small. However, it should be pointed out that the set $\{S, \Omega, y\}$ is not as good as $\{\nabla \bar{\mathbf{u}}, y\}$, although the two sets have essentially the same degree of freedom; it suggests that the model established by the ANN

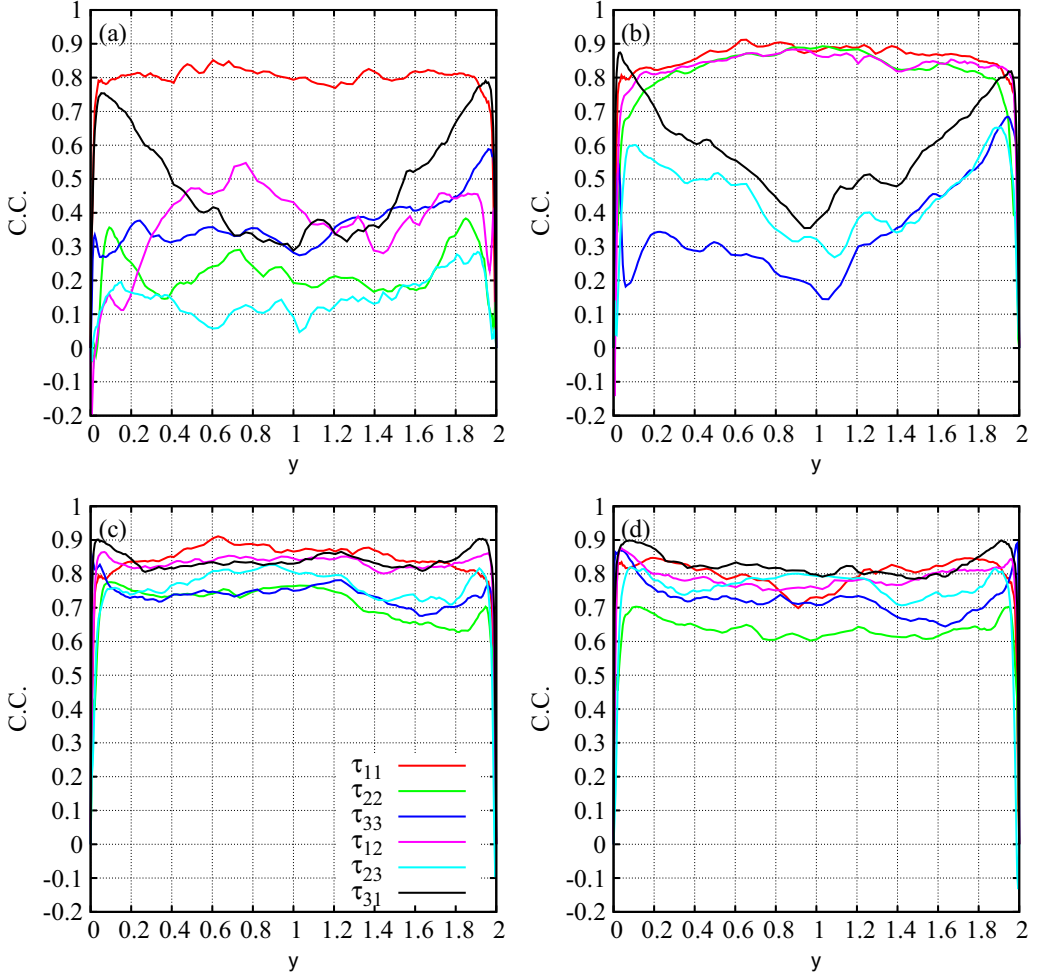


FIG. 4. Correlation coefficients between the SGS stress $\tau_{ij}^{(\text{DNS})}$ calculated using DNS data and $\tau_{ij}^{(\text{ANN})}$ predicted by trained ANN. Correlation coefficients are averaged in streamwise and spanwise directions (xz plane). $\text{Re}_\tau = 180$, $(\overline{\Delta x^+}, \overline{\Delta y_{\text{max}}^+}, \overline{\Delta z^+}) = (35.3, 9.9, 17.7)$. (a) $\{\mathbf{S}, y\}$, (b) $\{\mathbf{S}, \boldsymbol{\Omega}, y\}$, (c) $\{\nabla \bar{\mathbf{u}}, y\}$, and (d) $\{\nabla \bar{\mathbf{u}}\}$.

has simpler dependence on $\nabla \bar{\mathbf{u}}$ than on \mathbf{S} and $\boldsymbol{\Omega}$ as shown later in Sec. III E and tuning parameters of the ANN are required for successful learning.

Among the components of the SGS stress tensor τ_{11} is the easiest component for regression as all four sets give correlation coefficients larger than 0.7; this is because τ_{11} is largest in magnitude (Fig. 2). On the other hand, τ_{23} and τ_{31} , for which averages are zero and amplitudes are small (Fig. 2), are difficult to be approximated as the correlation coefficients are small for both $\{\mathbf{S}, y\}$ and $\{\mathbf{S}, \boldsymbol{\Omega}, y\}$. In the rest of the paper the set of input variables is fixed to $\{\nabla \bar{\mathbf{u}}, y\}$.

B. How successful is the learning?

Next, we look into some details of the learning results for $\text{Re}_\tau = 180$, $(\overline{\Delta x^+}, \overline{\Delta y_{\text{max}}^+}, \overline{\Delta z^+}) = (35.3, 9.9, 17.7)$. Figures 5 and 6 compare the distributions of the SGS stress obtained by filtering DNS data, $\tau_{ij}^{(\text{DNS})}$, and that predicted by trained ANN, $\tau_{ij}^{(\text{ANN})}$. We choose the plane $y = 0.1$ where the rms amplitudes of all components are nearly largest. The values of each component are normalized to

TABLE III. Correlation coefficients between the SGS stress $\tau_{ij}^{(\text{DNS})}$ calculated using DNS data and $\tau_{ij}^{(\text{ANN})}$ predicted by trained ANN. Correlation coefficients are averaged in the whole domain. $\text{Re}_\tau = 180, (\overline{\Delta x^+}, \overline{\Delta y_{\max}^+}, \overline{\Delta z^+}) = (35.3, 9.9, 17.7)$.

Input variables	τ_{11}	τ_{22}	τ_{33}	τ_{12}	τ_{23}	τ_{31}
$\{\mathcal{S}, y\}$	0.793	0.292	0.390	0.320	0.148	0.489
$\{\mathcal{S}, \boldsymbol{\Omega}, y\}$	0.776	0.769	0.344	0.773	0.368	0.524
$\{\nabla \bar{\mathbf{u}}, y\}$	0.804	0.713	0.728	0.791	0.730	0.821
$\{\nabla \bar{\mathbf{u}}\}$	0.767	0.670	0.710	0.776	0.720	0.820

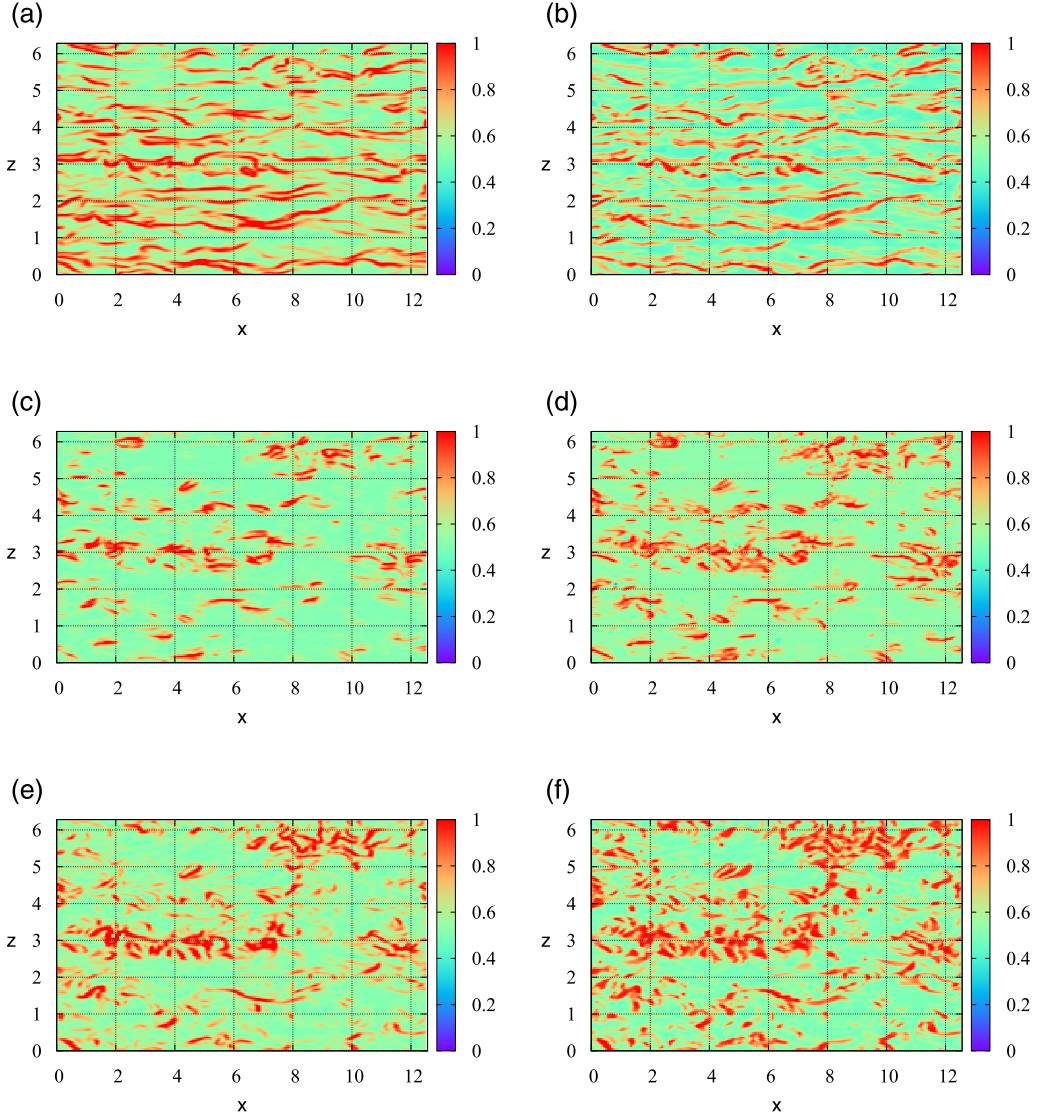


FIG. 5. Spatial distributions of SGS stress tensor at $y = 0.1$. Comparison between $\tau_{ij}^{(\text{DNS})}$ and $\tau_{ij}^{(\text{ANN})}$. Diagonal components. $\text{Re}_\tau = 180, (\overline{\Delta x^+}, \overline{\Delta y_{\max}^+}, \overline{\Delta z^+}) = (35.3, 9.9, 17.7)$. (a) $\tau_{11}^{(\text{DNS})}$, (b) $\tau_{11}^{(\text{ANN})}$, (c) $\tau_{22}^{(\text{DNS})}$, (d) $\tau_{22}^{(\text{ANN})}$, (e) $\tau_{33}^{(\text{DNS})}$, and (f) $\tau_{33}^{(\text{ANN})}$.

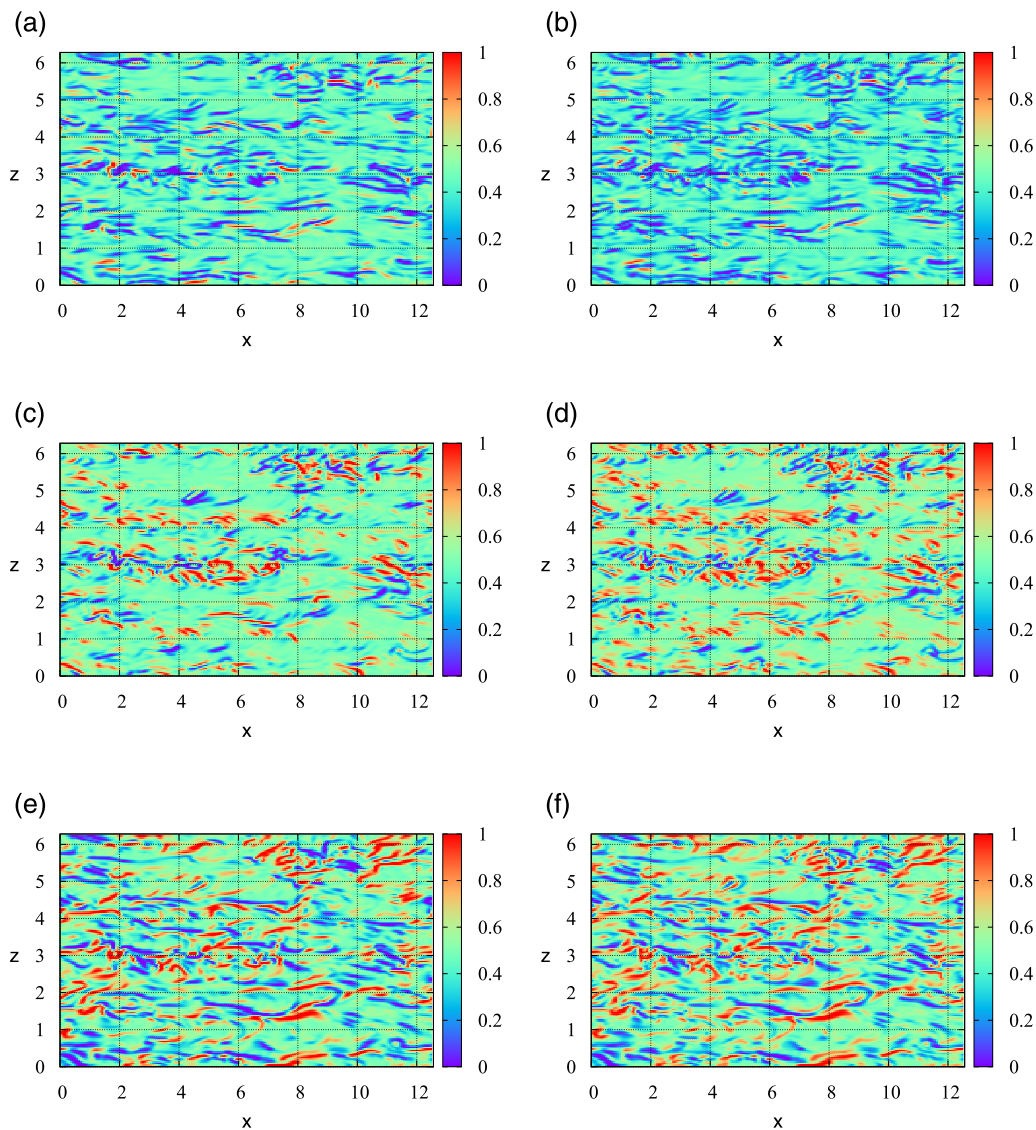


FIG. 6. Spatial distributions of SGS stress tensor at $y = 0.1$. Same as in Fig. 5 but for off-diagonal components. (a) $\tau_{12}^{(\text{DNS})}$, (b) $\tau_{12}^{(\text{ANN})}$, (c) $\tau_{23}^{(\text{DNS})}$, (d) $\tau_{23}^{(\text{ANN})}$, (e) $\tau_{31}^{(\text{DNS})}$, and (f) $\tau_{31}^{(\text{ANN})}$.

be in $[0, 1]$. The ANN is seen to reproduce fairly well the patterns in the distributions of DNS. Good agreement is also observed for the average (Fig. 7) and rms amplitude (Fig. 8) of each component. The learning is successful.

It is of interest to see whether the divergence of τ_{ij} , which appears in the momentum equation, can be predicted by the ANN. Figure 9 compares the distributions of $\partial_j \tau_{1j}$ between DNS and the trained ANN on the same plane as in Figs. 5 and 6. Again, ANN is seen to reproduce the patterns in the distributions of DNS. The correlation coefficients shown in Table IV are reasonably high, though they are slightly smaller than those of τ_{ij} .

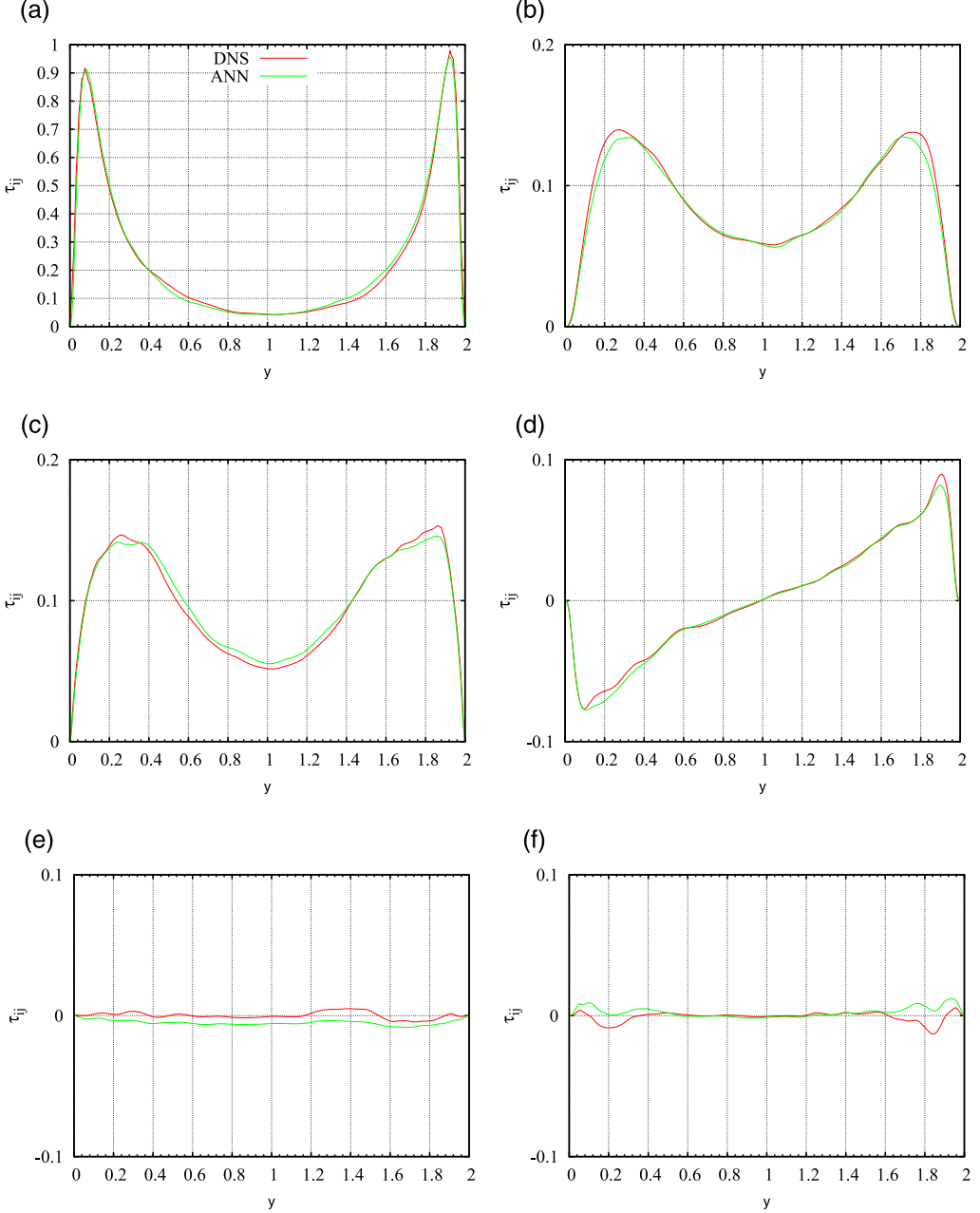


FIG. 7. SGS stress averaged in streamwise and spanwise directions. Comparison between $\tau_{ij}^{(\text{DNS})}$ and $\tau_{ij}^{(\text{ANN})}$. $\text{Re}_\tau = 180$, $(\overline{\Delta x^+}, \overline{\Delta y_{\text{max}}^+}, \overline{\Delta z^+}) = (35.3, 9.9, 17.7)$. (a) τ_{11} , (b) τ_{22} , (c) τ_{33} , (d) τ_{12} , (e) τ_{23} , and (f) τ_{31} .

C. Basic features of learning

In this section we show some features of learning by the ANN which can be important in efficient applications. Table V confirms that there is no significant dependence on the data set used in training. Five different data sets are tested. The difference between the correlation coefficients and the average is less than 0.043.

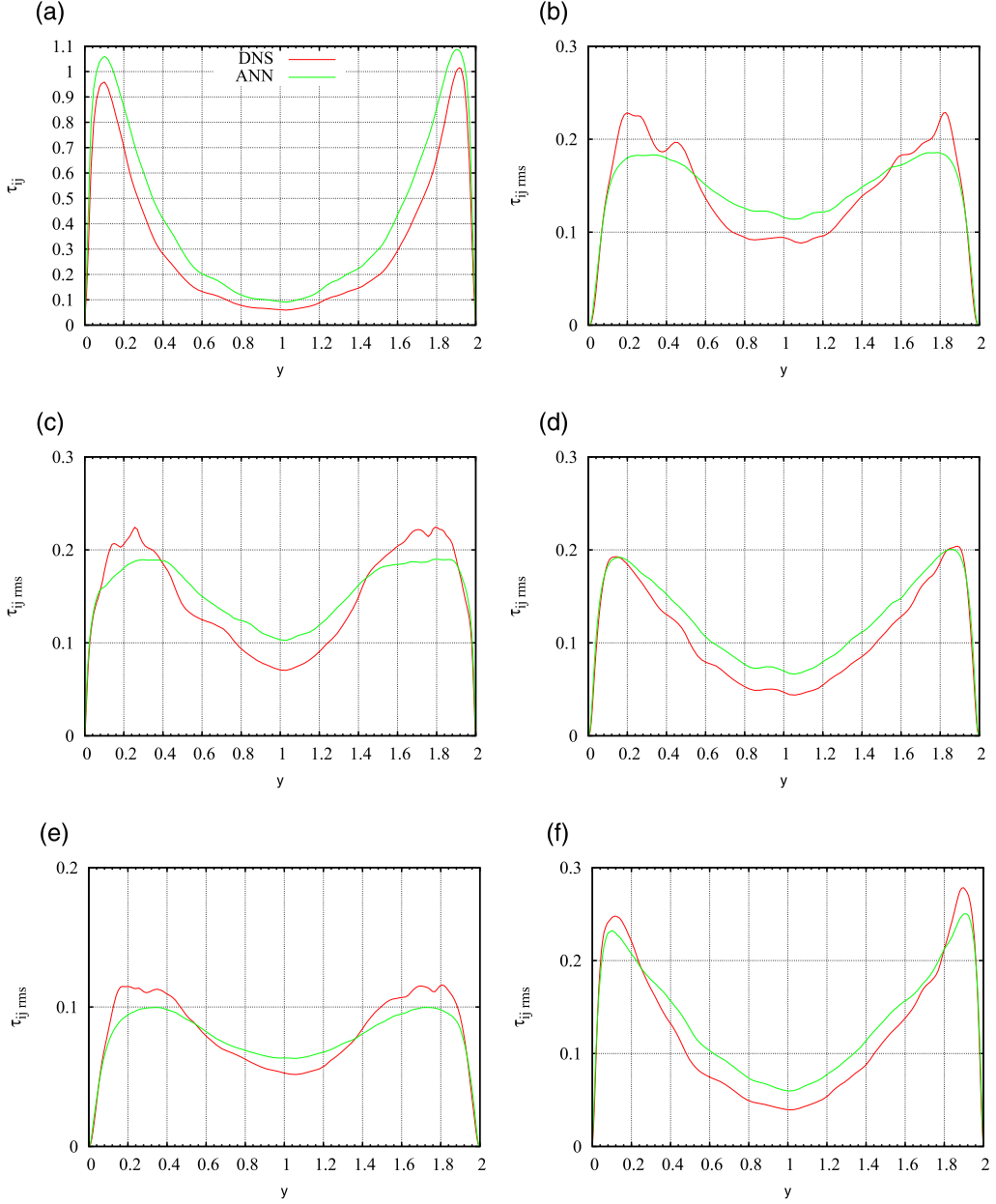


FIG. 8. The rms amplitude of fluctuation of SGS stress in streamwise and spanwise directions. Comparison between $\tau_{ij}^{(DNS)}$ and $\tau_{ij}^{(ANN)}$. $Re_\tau = 180$, $(\overline{\Delta x^+}, \overline{\Delta y_{max}^+}, \overline{\Delta z^+}) = (35.3, 9.9, 17.7)$. (a) τ_{11} , (b) τ_{22} , (c) τ_{33} , (d) τ_{12} , (e) τ_{23} , and (f) τ_{31} .

Figure 10 is a magnified view of Fig. 4 near the wall. It shows that the correlation coefficients are small in the near-wall region, $y^+ < 10$, which consists of the viscous sublayer and a part of the buffer layer; it is reasonable since the flow field is not fully turbulent in this region. Outside this region, however, the correlation coefficients do not depend on the position y significantly.

Table VI shows how many neurons are needed for successful learning. In this table n is the number of neurons in the hidden layer. In general, approximation by the ANN becomes more accurate by

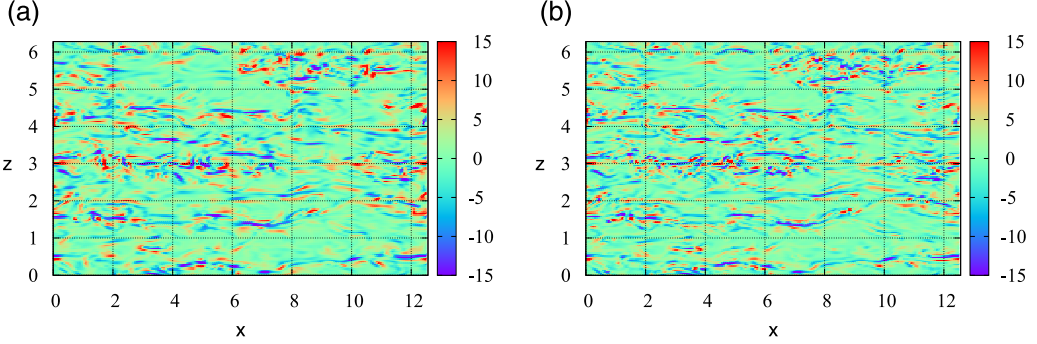


FIG. 9. Spatial distributions of divergence of SGS stress tensor at $y = 0.1$. Parameter values are the same as in Fig. 5. (a) $\partial_j \tau_{ij}^{(\text{DNS})}$ and (b) $\partial_j \tau_{ij}^{(\text{ANN})}$.

increasing n with the expense of computational time. It is seen that the correlation coefficients increase with n , but the increase is slow for $n \geq 10$. All correlation coefficients exceed 0.7 when $n \geq 50$. Figure 11 shows how the difference between DNS and ANN decays with the number of iterations in training. As the number of neurons increases, the rate of decay increases and the final error after 1000 iterations of learning decreases. On the other hand, the time required for ANN calculation increases with n . Thus the choice of n should be made by taking account of the accuracy of approximation as well as the calculation time.

Figure 12 shows the overall correlation coefficients as a function of the averaged filter size $\overline{\Delta}^+ = (\overline{\Delta x^+} \overline{\Delta y_{\max}^+} \overline{\Delta z^+})^{1/3}$ for various Reynolds numbers. It is seen that learning is successful for $\Delta^+ \lesssim 20$, which corresponds to about three to four times grid spacing. The correlation coefficients decrease quickly as the filter size becomes large. Thus there is a limitation for the filter size. There is little dependence on the Reynolds number, although the correlation coefficient is larger for $\text{Re}_\tau = 400$ than for the other three cases.

D. Applicability to higher Reynolds numbers

LES is usually used for high Reynolds number flows which are not accessible by DNS. Thus when we think of applying an ANN to LES of high Reynolds number flows, no training data are available from DNS. In this regard, it is of importance to check whether an ANN trained at low Reynolds numbers is useful at high Reynolds numbers. This is checked by applying an ANN trained at $\text{Re}_\tau = 180$ to predicting the SGS stress tensor at $\text{Re}_\tau = 400$ and 800. Figure 13 compares the distribution of $\tau_{11}^{(\text{DNS})}$ obtained by filtering DNS data of $\text{Re}_\tau = 400$ with filter size $(\overline{\Delta x^+}, \overline{\Delta y_{\max}^+}, \overline{\Delta z^+}) = (34.3, 17.9, 17.5)$ and $\tau_{11}^{(\text{ANN})}$ predicted by an ANN trained at $\text{Re}_\tau = 180$ with filter size $(\overline{\Delta x^+}, \overline{\Delta y_{\max}^+}, \overline{\Delta z^+}) = (35.3, 9.9, 17.7)$. Although there is some difference in the magnitude, the spatial patterns in DNS data are reproduced by the ANN. The correlation coefficients between DNS and the ANN are larger than 0.7 except for τ_{11} and τ_{12} at $\text{Re}_\tau = 800$ (Table VII). These results

TABLE IV. Correlation coefficients between the divergence of SGS stress $\partial_j \tau_{ij}^{(\text{DNS})}$ calculated using DNS data and $\partial_j \tau_{ij}^{(\text{ANN})}$ predicted by trained ANN. Correlation coefficients are averaged in the whole domain. $\text{Re}_\tau = 180$, $(\overline{\Delta x^+}, \overline{\Delta y_{\max}^+}, \overline{\Delta z^+}) = (35.3, 9.9, 17.7)$.

$\partial_j \tau_{1j}$	$\partial_j \tau_{2j}$	$\partial_j \tau_{3j}$
0.640	0.636	0.536

TABLE V. Correlation coefficients between the SGS stress $\tau_{ij}^{(DNS)}$ calculated using DNS data and $\tau_{ij}^{(ANN)}$ predicted by the trained ANN. Dependence on training data set. Correlation coefficients are averaged in the whole domain. $Re_\tau = 180$, $(\overline{\Delta x^+}, \overline{\Delta y_{max}^+}, \overline{\Delta z^+}) = (35.3, 9.9, 17.7)$.

Data set	τ_{11}	τ_{22}	τ_{33}	τ_{12}	τ_{23}	τ_{31}
1st	0.796	0.696	0.750	0.760	0.731	0.826
2nd	0.802	0.711	0.693	0.753	0.734	0.784
3rd	0.835	0.715	0.743	0.834	0.750	0.832
4th	0.768	0.709	0.708	0.792	0.732	0.826
5th	0.816	0.732	0.747	0.815	0.703	0.839
Average	0.804	0.713	0.728	0.791	0.730	0.821

TABLE VI. Correlation coefficients between $\tau_{ij}^{(DNS)}$ and $\tau_{ij}^{(ANN)}$. Dependence on the number of neurons. Correlation coefficients are averaged in the whole domain. $Re_\tau = 180$, $(\overline{\Delta x^+}, \overline{\Delta y_{max}^+}, \overline{\Delta z^+}) = (35.3, 9.9, 17.7)$.

n	τ_{11}	τ_{22}	τ_{33}	τ_{12}	τ_{23}	τ_{31}
2	0.677	0.487	0.486	0.366	0.398	0.547
5	0.752	0.671	0.674	0.593	0.604	0.710
10	0.742	0.672	0.717	0.779	0.711	0.801
25	0.782	0.684	0.739	0.807	0.736	0.807
50	0.806	0.709	0.739	0.796	0.739	0.812
100	0.827	0.711	0.739	0.788	0.736	0.816

TABLE VII. Correlation coefficients between $\tau_{ij}^{(DNS)}$ obtained by filtering DNS data of $Re_\tau = 400$ and 800 and $\tau_{ij}^{(ANN)}$ predicted by ANN trained at $Re_\tau = 180$ with filter size $(\overline{\Delta x^+}, \overline{\Delta y_{max}^+}, \overline{\Delta z^+}) = (35.3, 9.9, 17.7)$. The filter size is $(\overline{\Delta x^+}, \overline{\Delta y_{max}^+}, \overline{\Delta z^+}) = (34.3, 17.9, 17.5)$ for $Re_\tau = 400$ and $(\overline{\Delta x^+}, \overline{\Delta y_{max}^+}, \overline{\Delta z^+}) = (26.2, 10.9, 13.1)$ for $Re_\tau = 800$. Correlation coefficients are averaged in the whole domain.

Re_τ	τ_{11}	τ_{22}	τ_{33}	τ_{12}	τ_{23}	τ_{31}
400	0.707	0.744	0.734	0.743	0.768	0.769
800	0.694	0.767	0.739	0.672	0.764	0.773

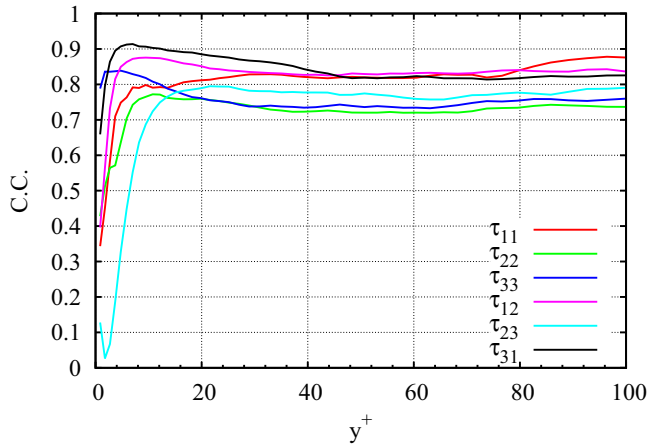


FIG. 10. Correlation coefficients between $\tau_{ij}^{(DNS)}$ and $\tau_{ij}^{(ANN)}$ in the near-wall region. Correlation coefficients are averaged in streamwise and spanwise directions. Magnified view of Fig. 4(c).

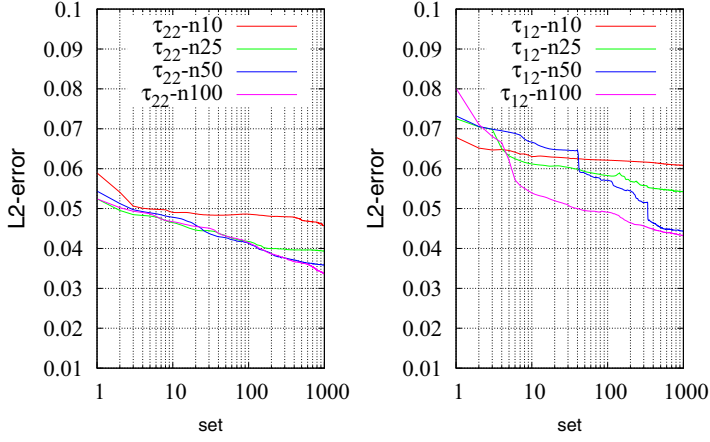


FIG. 11. L^2 norm of error between the output and the training target as a function of number of iterations. Left, τ_{22} ; right, τ_{12} . $\text{Re}_\tau = 180$, $(\overline{\Delta x^+}, \overline{\Delta y_{\max}^+}, \overline{\Delta z^+}) = (35.3, 9.9, 17.7)$.

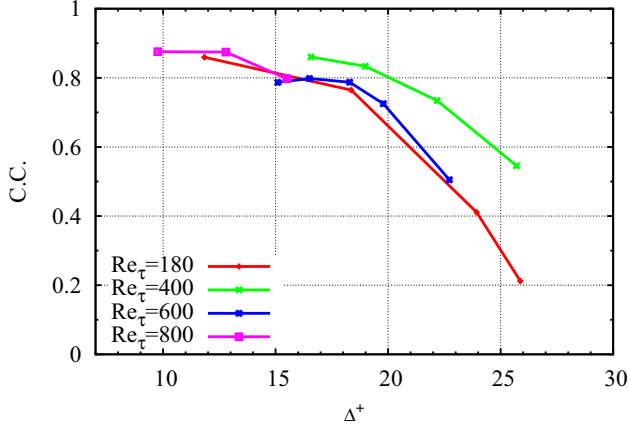


FIG. 12. Correlation coefficients between $\tau_{ij}^{(\text{DNS})}$ and $\tau_{ij}^{(\text{ANN})}$. Dependence on the filter size. Correlation coefficients are averaged in the whole domain. $\text{Re}_\tau = 180$, $(\overline{\Delta x^+}, \overline{\Delta y_{\max}^+}, \overline{\Delta z^+}) = (35.3, 9.9, 17.7)$.

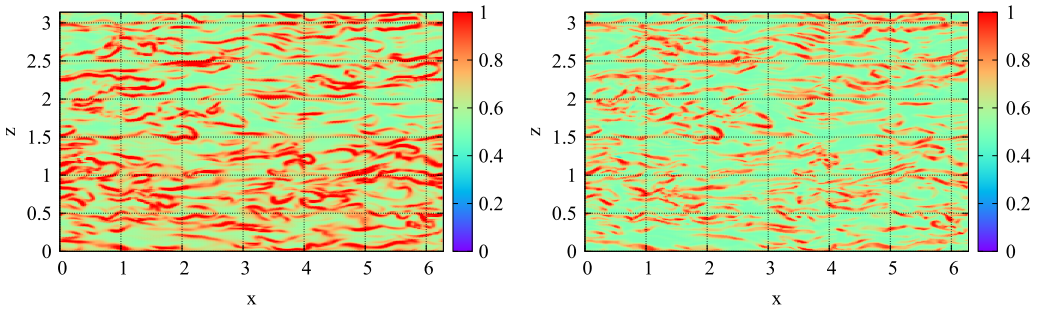


FIG. 13. Comparison between $\tau_{11}^{(\text{DNS})}$ obtained by filtering DNS data of $\text{Re}_\tau = 400$ with filter size $(\overline{\Delta x^+}, \overline{\Delta y_{\max}^+}, \overline{\Delta z^+}) = (34.3, 17.9, 17.5)$ and $\tau_{11}^{(\text{ANN})}$ predicted by the ANN trained at $\text{Re}_\tau = 180$ with filter size $(\overline{\Delta x^+}, \overline{\Delta y_{\max}^+}, \overline{\Delta z^+}) = (35.3, 9.9, 17.7)$. $y = 0.1$.

TABLE VIII. Input variables required for accurate prediction by the ANN.

	$\frac{\partial u}{\partial x}$	$\frac{\partial u}{\partial y}$	$\frac{\partial u}{\partial z}$	$\frac{\partial v}{\partial x}$	$\frac{\partial v}{\partial y}$	$\frac{\partial v}{\partial z}$	$\frac{\partial w}{\partial x}$	$\frac{\partial w}{\partial y}$	$\frac{\partial w}{\partial z}$
τ_{11}	○		○						
τ_{22}				○		○			
τ_{33}							○		○
τ_{12}	○		○						
τ_{23}				○		○	○		○
τ_{31}	○		○				○		○

support that it is possible to use an ANN trained at low Reynolds numbers for LES at high Reynolds numbers.

E. What has the ANN learned?

Here we investigate what kind of model the ANN has established. First, we identify and eliminate members of the input variables which are not required for ANN approximation for each component of the SGS stress tensor. This is done by removing components of $\nabla\bar{\mathbf{u}}$ one by one and checking whether the correlation coefficients become much smaller than before. Table VIII shows the results; the members of the input variables required for achieving high correlation coefficients are marked by circles. The values of correlation coefficients with the reduced numbers of input variables are shown in the first row of Table IX. They are larger than those obtained with the full members of $\{\nabla\bar{\mathbf{u}}, y\}$ (Table III). Thus the results of learning are improved by eliminating irrelevant components.

Next, we infer the model the ANN has produced. The above results imply that

$$\tau_{ij} = f\left(\frac{\partial\bar{u}_i}{\partial x}, \frac{\partial\bar{u}_i}{\partial z}, \frac{\partial\bar{u}_j}{\partial x}, \frac{\partial\bar{u}_j}{\partial z}, y\right), \quad (6)$$

which reminds us of the gradient model

$$\tau_{ij} = \frac{\bar{\Delta}^2}{12} \frac{\partial\bar{u}_i}{\partial x_k} \frac{\partial\bar{u}_j}{\partial x_k}. \quad (7)$$

We prefer the form

$$\tau_{ij} = \sum_{k=1}^3 \frac{\bar{\Delta}_k^2}{12} \frac{\partial\bar{u}_i}{\partial x_k} \frac{\partial\bar{u}_j}{\partial x_k}, \quad (8)$$

since the grid spacings in the y direction are much smaller than in the other two directions.

TABLE IX. Correlation coefficients between (i) $\tau_{ij}^{(\text{DNS})}$ and $\tau_{ij}^{(\text{ANN})}$ with reduced number of input variables, (ii) the gradient model and $\tau_{ij}^{(\text{DNS})}$, (iii) the gradient model and $\tau_{ij}^{(\text{ANN})}$, (iv) the Smagorinsky model and $\tau_{ij}^{(\text{DNS})}$, and (v) the Smagorinsky model and $\tau_{ij}^{(\text{ANN})}$. Correlation coefficients are averaged in the whole domain. $\text{Re}_\tau = 180$, $(\bar{\Delta x}^+, \bar{\Delta y}_{\text{max}}^+, \bar{\Delta z}^+) = (35.3, 9.9, 17.7)$.

Case	τ_{11}	τ_{22}	τ_{33}	τ_{12}	τ_{23}	τ_{31}
Reduced input variables	0.863	0.769	0.793	0.848	0.793	0.856
Gradient model vs DNS	0.847	0.729	0.737	0.841	0.703	0.853
Gradient model vs ANN	0.651	0.675	0.634	0.758	0.664	0.640
Smagorinsky vs DNS	0.257	0.134	-0.002	0.247	0.097	0.144
Smagorinsky vs ANN	0.199	0.152	-0.001	0.239	0.076	0.122

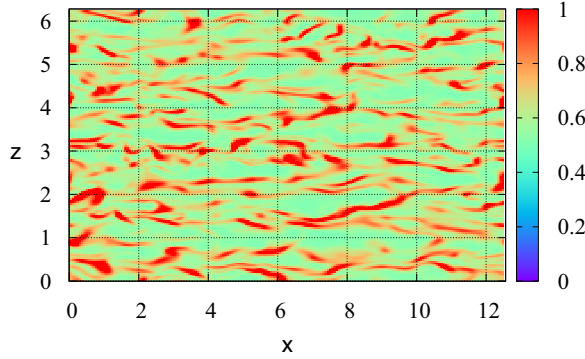


FIG. 14. Distribution of τ_{11} obtained by gradient model. $Re_\tau = 180$, $(\overline{\Delta x^+}, \overline{\Delta y_{\max}^+}, \overline{\Delta z^+}) = (35.3, 9.9, 17.7)$.

Figure 14 shows the distribution of τ_{11} obtained by the gradient model. It is similar to not only $\tau_{11}^{(\text{DNS})}$ but also $\tau_{11}^{(\text{ANN})}$ (Fig. 5). In Table IX the correlation between the gradient model (8) and DNS is high and comparable to the correlation between the ANN and DNS. The correlation coefficients between the gradient model and the ANN are a bit smaller than those in the first and second rows, but still large. Correlation with the Smagorinsky model is also included for comparison. As is well known, the Smagorinsky-type models have little correlation with DNS [27,28], which is confirmed in the fourth row of Table IX; it is also poorly correlated with the ANN. Thus, the ANN has established a model which is similar to the gradient model.

F. *A posteriori* test

Finally, actual LESs using the trained ANN are carried out to check the performance of the ANN model (*a posteriori* test). Table X lists the models and the parameters. Simulations using the Smagorinsky model are also carried out for comparison. The Van Driest damping is used in all LES calculations so that the boundary conditions are satisfied; the damping is introduced by simply multiplying the SGS stress by $(1 - e^{-y^+/A^+})^2$ with $A^+ = 25$. Two cases of DNS, $Re_\tau = 180$ and 400, are chosen (Table I). One limitation in the present study lies in the grid spacings in the y direction. Grid spacings should not be stretched significantly when we adopt the compact scheme, which has higher accuracy than the standard finite difference schemes like the second-order explicit finite difference; it is advised that the difference between neighboring grid spacings is kept lower than 5% [29]. In addition, the grid spacings should be small enough to capture the wall region since no numerical diffusion due to upwinding is introduced for stabilization. Thus the number of grid points in y cannot be reduced to the values listed in Table II, while the numbers of grid points in x and z are chosen from Table II. The ANN trained on the corresponding grids is used in cases ANN1 and ANN2. In case ANN3, however, the ANN trained on the grids $N_x \times N_y \times N_z = 84 \times 84 \times 84$

TABLE X. Parameter values for *a posteriori* test. Filter size and number of grid points.

Model (case)	Re_τ	$\overline{\Delta x^+}$	$\overline{\Delta y_{\max}^+}$	$\overline{\Delta z^+}$	$N_x \times N_y \times N_z$
ANN (ANN1)	180	35.3	9.9	17.7	$64 \times 64 \times 64$
ANN (ANN2)	400	29.9	14.2	15.0	$84 \times 120 \times 84$
ANN (ANN3)	400	39.3	14.2	19.6	$64 \times 120 \times 64$
Smagorinsky	180	35.3	9.9	17.7	$64 \times 64 \times 64$
Smagorinsky	400	29.9	14.2	15.0	$84 \times 120 \times 84$

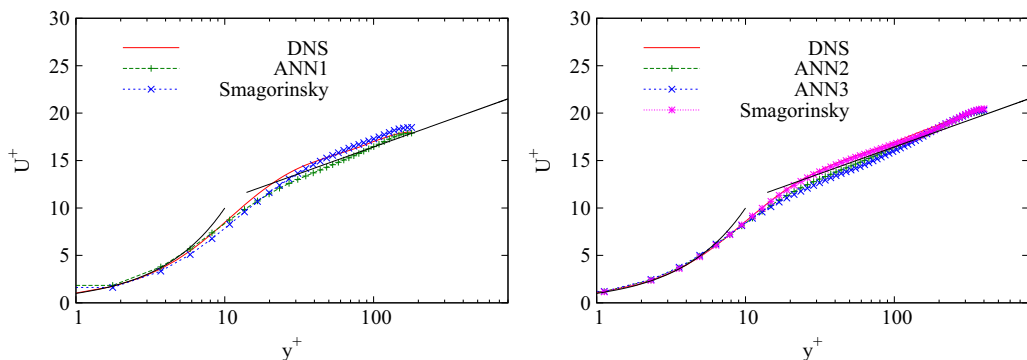


FIG. 15. Comparison of mean flow obtained by LES with Smagorinsky model and ANN model. Left, $Re_\tau = 180$; right, $Re_\tau = 400$.

is used with a factor adjusting the difference of grid spacings since correlation coefficients between $\tau_{ij}^{(DNS)}$ and $\tau_{ij}^{(ANN)}$ are not high on the grids $N_x \times N_y \times N_z = 64 \times 64 \times 64$ (Fig. 12).

Figure 15 compares the mean flow obtained by LES simulations. First of all, LES using the ANN models did not diverge and we could obtain mean flow and statistical quantities, while the gradient model is known to be unstable. The mean flow obtained by the Smagorinsky model is in reasonable agreement with DNS except that it is a bit underestimated for $10 \lesssim y^+ \lesssim 40$ at $Re_\tau = 180$. On the other hand, the mean flow obtained by the ANN model is smaller than DNS for $Re_\tau = 180$; deviation from the log law is observed for $20 \lesssim y^+ \lesssim 100$ at $Re_\tau = 400$. Although the difference is not so large, the ANN model has no advantage over the Smagorinsky model for prediction of the mean flow.

Figure 16 compares turbulence intensities obtained by filtering DNS, LES calculations with the Smagorinsky model, and the ANN model. In contrast to the mean flow there is no significant difference between filtered DNS and LES with ANN models, while ANN slightly overpredicts $\langle \bar{v}^2 \rangle_{xz}^{1/2}$ and $\langle \bar{w}^2 \rangle_{xz}^{1/2}$ at $Re_\tau = 180$. These results imply that ANN can be a promising tool for searching for new turbulence models, although further improvement and verification should be followed.

IV. CONCLUDING REMARKS

We have shown that an ANN can establish a functional relation between the GS flow field and the SGS stress tensor in LES. Using DNS data of a turbulent channel flow as training data, the ANN was trained by back-propagation. Then the ability of the trained ANN was tested using DNS data which were not used in training. Learning was most successful when $\{\nabla \bar{u}, y\}$ was used as a set of the input variables; the correlation coefficients between the SGS stress tensor obtained by filtering DNS data and that predicted by ANN exceeded 0.7. The spatial distribution of the SGS stress tensor predicted by the ANN was in good agreement with that obtained by filtering DNS data. It is most likely that the ANN has established a model close to the gradient model. An *a posteriori* test using the trained ANN was also carried out. Although the ANN model showed no advantage over the Smagorinsky model, the results obtained using ANN models were not far from those of DNS, suggesting that further improvement will establish a new model that can be used for actual LES calculations.

It should be pointed out that learning was successful only when the filter size was small: $\bar{\Delta}^+ \lesssim 20$. For this small filter size the SGS Reynolds stress term is so small that the SGS stress is close to the sum of the Leonard term and the cross-stress term, which can be approximated by the gradient model. Therefore, the present results are quite reasonable. However, it should be stressed that the ANN has succeeded in establishing a functional relation between the GS flow field and the SGS stress without any assumption on the form of function. We also remark that the values of correlation

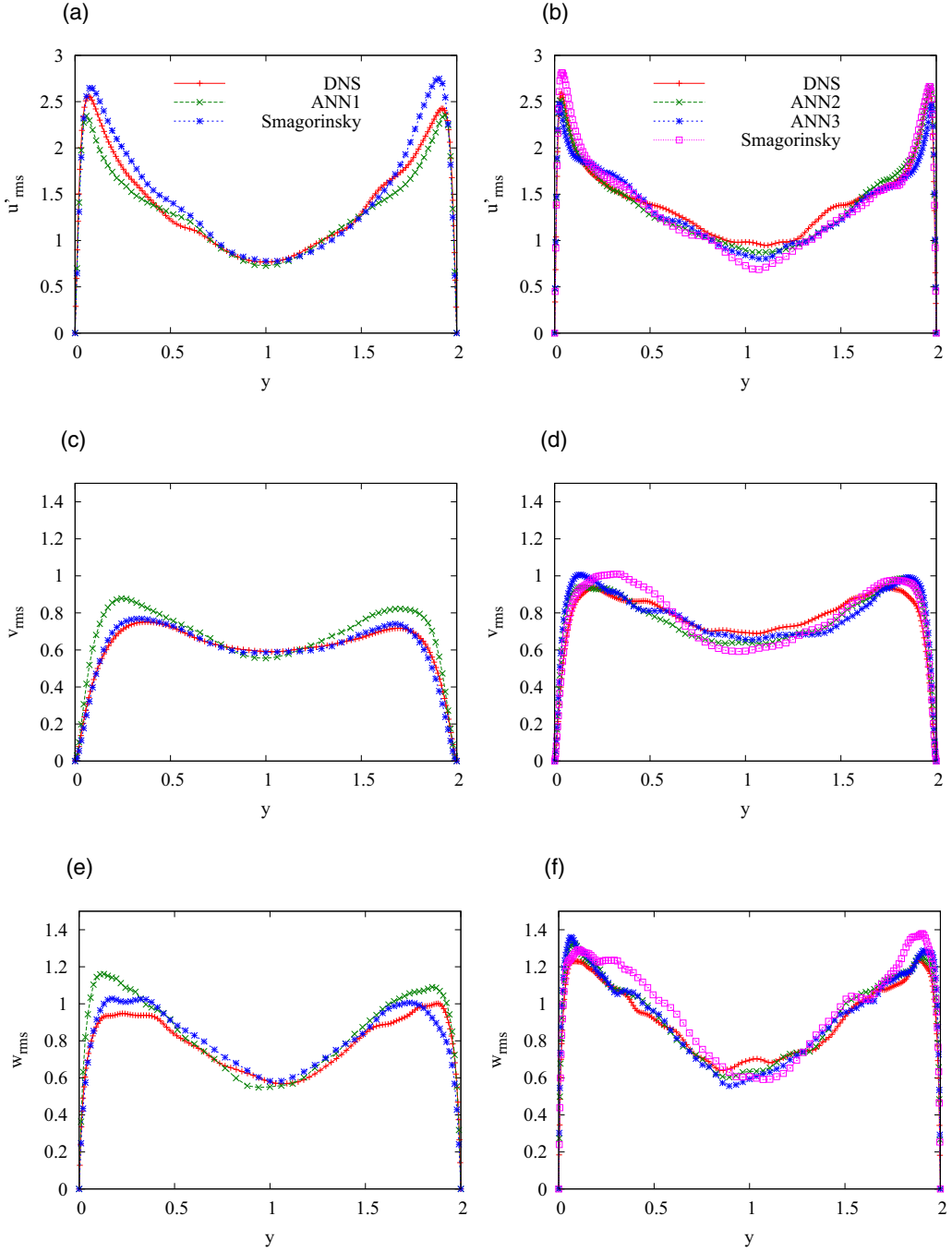


FIG. 16. GS turbulence intensities. Comparison between DNS and LES with the Smagorinsky model and the ANN model. $Re_\tau = 180$ and 400 . (a) $\langle \bar{u}^2 \rangle_{xz}^{1/2}$, $Re_\tau = 180$, (b) $\langle \bar{u}^2 \rangle_{xz}^{1/2}$, $Re_\tau = 400$, (c) $\langle \bar{v}^2 \rangle_{xz}^{1/2}$, $Re_\tau = 180$, (d) $\langle \bar{v}^2 \rangle_{xz}^{1/2}$, $Re_\tau = 400$, (e) $\langle \bar{w}^2 \rangle_{xz}^{1/2}$, $Re_\tau = 180$, and (f) $\langle \bar{w}^2 \rangle_{xz}^{1/2}$, $Re_\tau = 400$.

coefficients between DNS and the ANN obtained in the present study are comparable to or even larger than those for similarity models [26,30] but smaller than those for a dynamic two-parameter

mixed model [28], which implies that the ANN is a promising tool for searching for new turbulence models and should be improved.

In the present study we have not taken care of symmetry of the SGS stress tensor; each component of the tensor is trained separately. If the fluctuations are statistically isotropic, however, the turbulence model should be also isotropic; training is required for only one diagonal component and one off-diagonal component of the SGS stress tensor, while the two are related through the incompressibility condition. In the present study, however, the grid spacings and the filter size differ depending on the direction; this is one of the reasons why each component of the SGS stress tensor is trained independently. It should be noted that it is important to take account of symmetry when we formulate a trained ANN into a turbulence model. Another limitation in the present study is that each training is performed using data with fixed filter size. As a result dependence on the filter size cannot be incorporated into the ANN model. To do this data with different filter size should be used together as training data and filter size should be included in the input variables, which demand more computational resources.

Although we have obtained some successful results with ANN, several problems should be solved in order to find a new turbulence model better than the existing ones, which is our final goal. We would like to find a model which works well even when the filter size is much larger than the grid size. However, it may be impossible to have high correlation of the SGS stress tensor between the ANN and DNS for large filter size since SGS fluctuations involve a wide range of length scales and are inevitably large. In this regard, one way to proceed is to allow a certain level of errors, which can be incorporated in other methods of machine learning like support vector machine and regression. Another way is to replace the training target or output variable; in the present study we chose the SGS stress tensor as the output variable, but it is sometimes argued that high correlation of the SGS stress tensor is not necessary for an SGS model to be successful [12], although some models with high correlation coefficients are also successful [28]. The training target can be other quantities like the rate of production of residual energy or SGS dissipation, which is important in the energy transfer between GS and SGS scales.

The ANN itself should be also improved. There are a number of possibilities in the choice of input variables. In the present study the input variables were chosen by taking account of the Smagorinsky model, but it can be replaced by the similarity model and we can include doubly filtered variables in the input variables. We may include all data if the ability of the ANN allows it. In this regard, tuning of the ANN would be also important; the number of layers may be increased as we see the remarkable success of deep learning.

ACKNOWLEDGMENT

Numerical calculations were performed on the Altix UV1000 and UV2000 at the Advanced Fluid Information Research Center, Institute of Fluid Science, Tohoku University.

-
- [1] J. Smagorinsky, General circulation experiments with the primitive equations, *Mon. Weather Rev.* **91**, 99 (1963).
 - [2] J. Bardina, J. H. Ferziger, and W. C. Reynolds, Improved turbulence models based on large eddy simulation of homogeneous, incompressible, turbulent flows, Report No. TF-19, Department of Mechanical Engineering, Stanford University (1983).
 - [3] R. A. Clark, J. H. Ferziger, and W. C. Reynolds, Evaluation of subgrid-scale models using an accurately simulated turbulent flow, *J. Fluid Mech.* **91**, 1 (1979).
 - [4] M. Germano, Turbulence: The filtering approach, *J. Fluid Mech.* **238**, 325 (1992).
 - [5] B. Vreman, B. Geurts, and H. Kuerten, Large eddy simulation of the temporal mixing layer using the Clark model, *Theor. Comput. Fluid Dyn.* **8**, 309 (1996).
 - [6] Y. Zang, R. L. Street, and J. R. Koseff, A dynamic mixed subgrid-scale model and its application to turbulent recirculating flows, *Phys. Fluids A* **5**, 3186 (1993).

- [7] M. Lesieur and O. Métais, New trends in large-eddy simulations of turbulence, *Annu. Rev. Fluid Mech.* **28**, 45 (1996).
- [8] C. Meneveau and J. Katz, Scale-invariance and turbulence models for large-eddy simulation, *Annu. Rev. Fluid Mech.* **32**, 1 (2000).
- [9] C. Fureby, G. Tabor, H. G. Weller, and A. D. Gosman, A comparative study of subgrid scale models in homogeneous isotropic turbulence, *Phys. Fluids* **9**, 1416 (1997).
- [10] B. Vreman, B. Geurts, and H. Kuerten, Large-eddy simulation of the turbulent mixing layer, *J. Fluid Mech.* **339**, 357 (1997).
- [11] F. Hamba, Nonlocal analysis of the Reynolds stress in turbulent shear flow, *Phys. Fluids* **17**, 115102 (2005).
- [12] S. B. Pope, *Turbulent Flows* (Cambridge University Press, New York, 2002).
- [13] F. Sarghini, G. de Felice, and S. Santini, Neural networks based subgrid scale modeling in large eddy simulations, *Comput. Fluids* **32**, 97 (2003).
- [14] A. Moreau, O. Teytaud, and J. P. Bertoglio, Optimal estimation for large-eddy simulation of turbulence and application to the analysis of subgrid models, *Phys. Fluids* **18**, 105101 (2006).
- [15] M. Ma, J. Lu, and G. Tryggvason, Using statistical learning to close two-fluid multiphase flow equations for a simple bubbly system, *Phys. Fluids* **27**, 092101 (2015).
- [16] M. Ihme, C. Schmitt, and H. Pitsch, Optimal artificial neural networks and tabulation methods for chemistry representation in LES of a bluff-body swirl-stabilized flame, *Proc. Combust. Inst.* **32**, 1527 (2009).
- [17] B. A. Sen and S. Menon, Turbulent premixed flame modeling using artificial neural networks based chemical kinetics, *Proc. Combust. Inst.* **32**, 1605 (2009).
- [18] B. A. Sen, E. R. Hawkes, and S. Menon, Large eddy simulation of extinction and reignition with artificial neural networks based chemical kinetics, *Combust. Flame* **157**, 566 (2010).
- [19] M. D. Emami and A. E. Fard, Laminar flamelet modeling of a turbulent CH₄/H₂/N₂ jet diffusion flame using artificial neural networks, *Appl. Math. Model.* **36**, 2082 (2012).
- [20] J. Citrin, S. Breton, F. Felici, F. Imbeaux, T. Aniel, J.F. Artaud, B. Baiocchi, C. Bourdelle, Y. Camenen, and J. Garcia, Real-time capable first principle based modelling of tokamak turbulent transport, *Nucl. Fusion* **55**, 092001 (2015).
- [21] J. Kim, P. Moin, and R. Moser, Turbulence statistics in fully developed channel flow at a low Reynolds number, *J. Fluid Mech.* **177**, 133 (1987).
- [22] H. Abe, H. Kawamura, and Y. Matsuo, Direct numerical simulation of a fully developed turbulent channel flow with respect to the Reynolds number dependence, *Trans. ASME J. Fluids Eng.* **123**, 382 (2001).
- [23] W. Schoppa and F. Hussain, Coherent structure generation in near-wall turbulence, *J. Fluid Mech.* **453**, 57 (2002).
- [24] B. Ganapathisubramani, E. K. Longmire, and I. Marusic, Experimental investigation of vortex properties in a turbulent boundary layer, *Phys. Fluids* **18**, 055105 (2006).
- [25] H. Kobayashi, The subgrid-scale models based on coherent structures for rotating homogeneous turbulence and turbulent channel flow, *Phys. Fluids* **17**, 045104 (2005).
- [26] S. Liu, C. Meneveau, and J. Katz, On the properties of similarity subgrid-scale models as deduced from measurements in a turbulent jet, *J. Fluid Mech.* **275**, 83 (1994).
- [27] M. V. Salvetti and S. Banerjee, A priori tests of a new dynamic subgrid-scale model for finite-difference large-eddy simulations, *Phys. Fluids* **7**, 2831 (1995).
- [28] K. Horiuti, A new dynamic two-parameter mixed model for large-eddy simulation, *Phys. Fluids* **9**, 3443 (1997).
- [29] B. E. Mitchell, S. K. Lele, and P. Moin, Direct computation of the sound from a compressible co-rotating vortex pair, *J. Fluid Mech.* **285**, 181 (1995).
- [30] K. Horiuti, The role of the Bardina model in large eddy simulation of turbulent channel flow, *Phys. Fluids A* **1**, 426 (1989).